# Deep neural network prediction for effective thermal conductivity and spreading thermal resistance for flat heat pipe

Myeongjin Kim

*Department of Hydrogen and Renewable Energy,
Kyungpook National University, Daegu, Republic of Korea, and*

Joo Hyun Moon

*Department of Mechanical and Aerospace Engineering,
Sejong University, Seoul, Republic of Korea*

## Abstract

**Purpose** – This study aims to introduce a deep neural network (DNN) to estimate the effective thermal conductivity of the flat heat pipe with spreading thermal resistance.

**Design/methodology/approach** – A total of 2,160 computational fluid dynamics simulation cases over up to 2,000 W/mK are conducted to regress big data and predict a wider range of effective thermal conductivity up to 10,000 W/mK. The deep neural networking is trained with reinforcement learning from 10–12 steps minimizing errors in each step. Another 8,640 CFD cases are used to validate.

**Findings** – Experimental, simulational and theoretical approaches are used to validate the DNN estimation for the same independent variables. The results from the two approaches show a good agreement with each other. In addition, the DNN method required less time when compared to the CFD.

**Originality/value** – The DNN method opens a new way to secure data while predicting in a wide range without experiments or simulations. If these technologies can be applied to thermal and materials engineering, they will be the key to solve thermal obstacles that many longing to overcome.

**Keywords** Computational fluid dynamics, Effective thermal conductivity, Flat heat pipe, Neural network, Thermal system design

**Paper type** Research paper

## Nomenclature

$A_c$ = heatsink area, m$^2$;
$A_h$ = heater area, m$^2$;
$A_i$ = interfacial material area, m$^2$;
$Bi$ = Biot number;

$b$ = bias function;
CFD = Computational fluid dynamics;
DNN = Deep neural network;
$d_c$ = equivalent heatsink diameter, m;
$d_h$ = equivalent heat source diameter, m;
$E$ = entalphy, J;
$f$ = activation function.
$g$ = thermal resistance function;
$h$ = heat transfer coefficient, W/m$^2$K;
$k_{eff}$ = effective thermal conductivity, W/mK;
$MAPE$ = mean absolute percentage error, %;
$N$ = number of data point;
$Q$ = heat power, W;
$q''$ = heat flux, W/m$^2$;
$ReLU$ = rectified linear unit;
$RMSE$ = root mean square error, K/W;
$R$ = spreading thermal resistance, calculated with CFD, K/W;
$R_{Cu}$ = spreading thermal resistance of copper by measurement, K/W;
$R_c$ = thermal resistance of heatsink by measurement, K/W;
$R_{DNN}$ = spreading thermal resistance, estimated with DNN, K/W;
$R_{est}$ = spreading thermal resistance, estimated equation (14), K/W;
$R_h$ = thermal resistance of heater by measurement, K/W;
$R_i$ = thermal resistance of interfacial material by measurement, K/W;
$R_{SNN}$ = spreading thermal resistance, estimated with SNN, K/W;
SNN = Shallow neural network;
$Tanh$ = hyper tangent function;
$\overline{T}_h$ = average heat source temperature, K or °C;
$\overline{T}_c$ = average heat source temperature, K or °C;
$T$ = temperature, K or °C;
$T_{mc}$ = heatsink temperature by measurement, K or °C;
$T_{mh}$ = heater temperature by measurement, K or °C;
$t$ = thickness, m;
$t_c$ = distance between heatsink surface and thermocouple, m;
$t_h$ = distance between heater surface and thermocouple, m;
$t_i$ = thickness of interfacial material, m;
$w$ = weight for input value;
$x$ = input value;
$y$ = output value by simulation;
$\hat{y}$ = output value by neural network; and
$z$ = weighted output value.

*Greek symbols*
$\varepsilon$ = dimensionless heat source radius, $d_h/d_c$;
$\lambda$ = dimensionless parameter, $\pi + 1/(\sqrt{\pi}\varepsilon)$;
$\rho$ = density, kg/m$^3$;
$\tau$ = dimensionless plate thickness, $t/d_c$; and
$\Phi$ = dimensionless parameter, $-$.

## 1. Introduction

Developing an optimal thermal design for an electric vehicle or a computer chip is critical as the need for them has risen, but the lifetime of devices shortens with use (Lewis *et al.*, 1996; Lewis, 2004, 2016). Their temperature needs to be controlled to stay in the desirable range. Therefore, the demand for thermal engineering has gone up (Navti *et al.*, 1997; Lewis and Sukirman, 1994; Teimouri and Behzadmehr, 2020). A conductive device for a heat sink is studied to lower the temperature. Vapor chamber, heat spreader, heat pipe and thermal ground plane have been shown to be excellent examples of substituting copper solids because they have a higher effective thermal conductivity (Bar-Cohen *et al.*, 2015; Chang and Hung, 2019). A flat heat pipe is wide but thin. The heat from a small-size heater can be delivered to a large heatsink area. Due to the nature of the flat heat pipe, the high spreading thermal resistance is inevitably generated. Heat pipe design should aim at lowering the spreading thermal resistance.

There are many variations, such as the flat heat pipe (Chen *et al.*, 2019; Zhu *et al.*, 2020), vapor chamber (Liu *et al.*, 2018; Zhou *et al.*, 2019; Yang *et al.*, 2021), thermal ground plane (Moon *et al.*, 2021b) and heat spreader (Tsai *et al.*, 2013), used to minimize the spreading thermal resistance. In this study, these variations are united "the flat heat pipe". A small amount of working fluid, such as DI water, flows in a flat pipe to allow phase change heat transfer from boiling to condensation. Also, a higher convective heat transfer by the working fluid can be added (Moon *et al.*, 2021a). However, when designing a thermal system, wick or rib structures in the flat heat pipe are not the primary consideration. Regardless of the internal shape, heat pipes look similar outside. They can be square or rectangular for convenience. Their thickness is usually within 5 mm. (Liu *et al.*, 2018). To optimize the thermal design, heatsink area, thickness, heater area and effective thermal conductivity are key parameters. More research is required to link the actual thermal system design to the flat heat pipe. However, applying the parameters of the spreading thermal resistance to the actual cooling devices is complex in estimating the effective thermal conductivity.

Many kinds of literature on the flat heat pipe have investigated effective thermal conductivity under different conditions. Zhou *et al.* (2019) showed the effective thermal conductivity model of copper vapor chambers. The spatial distribution of temperature was reported for different effective thermal conductivities. They also compared the thermal conductivity model with fabricated vapor chambers with different wick structures. Zhu *et al.* (2020) obtained a correlation of the effective thermal conductivity of a flat heat pipe. Effective thermal conductivity with different sizes were predicted based on the measured thermal resistance. Wang (2010) introduced a vapor chamber concept replacing the metal base plate, a multiphase heat transfer between water and vapor to apply to the graphic processing unit (GPU) of a smaller area with high power density. The optimal total thermal resistance of the vapor chamber is obtained with different power densities. Yang *et al.* (2021) introduced an effective thermal conductivity model for an ultrathin vapor chamber. Integration of hydrophilic and hydrophobic surfaces inside the chamber allowed a lower spreading thermal resistance and a calculated effective thermal conductivity up to 11,915 W/mK. The literatures discussed above mentioned an effective thermal conductivity model related to the spreading thermal resistance. The models have not reflected the conduction and convection heat transfer. The correlative models on the effective thermal conductivity were based on the bulk thermal resistance (Lee *et al.*, 1995; Song *et al.*, 1994), considering only the morphology. As the temperature distribution of a solid changes depending on the convective heat transfer of heatsink, this physics should be comprehensively considered. For example, the bulk material resistance reaches the order of $10e^{-6}$ K/W, which is quite smaller than the estimated value of spreading thermal resistance

of the order of 0.1 K/W (Lee *et al.*, 1995; Song *et al.*, 1994; Moon *et al.*, 2021b), leading to an overestimation.

For the flat heat pipe, it is known that a high temperature is expected at the heater, and a lower temperature is measured at the heatsink (Zhou *et al.*, 2019). It is hard to measure the effective thermal conductivity in experiments, but a conduction and convection heat transfer can be estimated simultaneously using a simulation tool that model the parameter correctly. Moon *et al.* (2021b) used the computational fluid dynamics (CFD) to show the correlation between the effective thermal conductivity and spreading thermal resistance. However, a small sample of the simulation was reported to a heater $10 \times 10$ mm$^2$ in size and a heatsink of $80 \times 80$ mm$^2$, and a single size was used for a small range of effective thermal conductivity. Various sizes of the flat heat pipes should be studied to analyze the spreading thermal resistance and effective thermal conductivity up to 10,000 W/mK. Zhou *et al.* (2019), Zhu *et al.* (2020) and Yang *et al.* (2021) reported the high effective thermal conductivity.

Recently, machine learning with a neural network has been rigorously used to get a more accurate regression model on the effective thermal conductivity or other crucial parameters of the thermal systems. Jamei *et al.* (2021) predicted the thermal conductivity of nanofluids with a neural network. Using 400 data sets, the classification map of the effective thermal conductivity of nanofluid was presented for the shallow neural network (SNN) and neural network with the filter training algorithm. Jiang and Zhao (2013) predicted the critical heat flux of the flow boiling phenomena using a neural network from 513 to 24,781 data sets. The SNN and hybrid neural network model with statistical learning theory were compared. Lee *et al.* (2020) provided the hidden layer effect on the prediction of heating energy consumption in old houses. The accuracy improved as the number of hidden layers increased when studied with 16,158 data sets. What neural network modelings have in common is that their prediction accuracy rose along with the number of datapoints. More studies are needed to investigate the relationship between the shallow or deep network architectures and the number of data sets, as there is still a lack of research on thermal system design, particularly with the flat heat pipe. Future works should look at the number of data sets required for neural network modeling suitable for thermal system design.

Therefore, the major objective of this investigation is to estimate the effective thermal conductivity of flat heat pipes of different morphologies and operating conditions by using a deep neural network (DNN) model. For flat heat pipe (FHP), it is a multi-linear case which is not dominated by a single variable. The DNN model first learns CFD data and then comes up with a new DNN model in steps. When a new DNN model is developed, the thermal resistance $R$ can be predicted when a new input variable ($k_{eff}$, $A_c$, $A_h$, $t$ and $h$) is given.

We will first obtain the big data in a specific range via CFD results ($100 \le k_{eff} \le 2,000$ W/mK, where $k_{eff}$ is effective thermal conductivity), then the DNN regression proceeds to predict in a range broader by five times ($2,000 \le k_{eff} \le 10,000$ W/mK). Validation via CFD will also be performed for the same range ($2,000 \le k_{eff} \le 10,000$ W/mK). When the models from the DNN and CFD results are compared, the difference is small. When compared with Lee *et al.*'s mathematical model (Lee *et al.*, 1995), the DNN result is a good fit. In conclusion, the DNN method opens a new way to secure data while predicting in a wide range without experiments or simulations. If this technology can be applied to thermal and materials engineering, they will be the key to solve thermal obstacles that many longing to overcome.

## 2. Numerical methods

### 2.1 Computational fluid dynamics
Ansys Fluent is used in this study to investigate the flat heat pipe with various effective thermal conductivities on the basis of the straightforward and generic model shown in

Figure 1. A flat heat pipe is investigated without considering gravity. Heating areas, $A_h$, have $10 \times 10$ mm$^2$ and $25 \times 25$ mm$^2$. In addition, flat heat pipes are selected to simulate heatsinks with different sizes, $A_c$, including $60 \times 60$ mm$^2$, $90 \times 90$ mm$^2$ and $120 \times 120$ mm$^2$. A detailed simulation input map is shown in Table 1. Thermal conductivity increasing by 100 W/mK, from 100 W/mK to 10,000 W/mK, are used with three heat transfer coefficients (100 W/m$^2$K, 500 W/m$^2$K and 1,000 W/m$^2$K). Heat inputs at the heater are fixed as 1 MW/m$^2$. Various thicknesses are adopted to cover flat heat pipes used in real applications. Therefore, a total of 10,800 cases ($2 \times 3 \times 100 \times 3 \times 6$) run in a row using Fluent. For the regression learning in a neural network, 2,160 simulations with effective thermal conductivity ranging from 100 to 2,000 W/mK are used. The rest of 8,640 cases are used for validation with DNN.

The three-dimensional and steady-state conditions are used. The uniform convective heat transfer $h$ is applied to reflect the actual heatsink specifications. The cold plate using the water circulation has $h$ of $\sim$ 1,000 W/m$^2$K, when $R \sim 1/hA_c$ and a heatsink with air cooling is the order of $h \sim 100$ W/m$^2$K (Lee *et al.*, 1995; Moon *et al.*, 2021b; Zhou *et al.*, 2019). With the heatsink, the ambient temperature is 25°C, where sidewalls are insulated. Grid dependency tests are made to from 3,000,000 to 10,000,000 hexagonal cells. At the heatsink, the heat transfer coefficient is evenly set, and the reference temperature is set as 40°C.

The thermophysical properties are presumed to be steady at different temperature conditions, and the density (8,900 kg/m$^3$) and specific heat (390 J/kgK) are set as same as copper. For mass conservation in CFD, the equations for the steady-state are used (Ansys, 2022; Lewis *et al.*, 1996; Lewis, 2004, 2016):
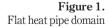
$$\nabla \cdot \left( \rho \, \overrightarrow{v} \right) = 0, \tag{1}$$

where there is no source term in equations (1) and (2). The energy conservation equation is used to solve the conduction heat transfer:



**Heater:**
$10 \times 10$ mm$^2$ / $25 \times 25$ mm$^2$
$q'' = 1,000$ kW/m$^2$

$k_{eff} = [100 - 10,000]$ W/mK

$t = 0.5 \sim 5.0$ mm

**Heat Sink:**
$60 \times 60$ mm$^2$ / $90 \times 90$ mm$^2$ / $120 \times 120$ mm$^2$
$h = [100 - 1,000]$ W/m$^2$K

Figure 1.
Flat heat pipe domain

| Cases | | | $A_c$ (3 cases) | |
|---|---|---|---|---|
| | | $60 \times 60$ mm$^2$ | $90 \times 90$ mm$^2$ | $120 \times 120$ mm$^2$ |
| $A_h$ (2 cases) | $10 \times 10$ mm$^2$ $25 \times 25$ mm$^2$ | | $k_{eff} = [100{:}100{:}10{,}000$ W/mK] (100 cases) and $t = [0.5, 1, 2, 3, 4, 5]$ mm (6 cases) and $h = 100$ W/m$^2$K, 500 W/m$^2$K and 1,000 W/m$^2$K (3 cases) | |

Table 1.
Simulation overview

$$\nabla \cdot (k_{\text{eff}} \nabla T) = \nabla \cdot (\rho \, \vec{v} E), \tag{2}$$

where $k_{\text{eff}}$ is the effective thermal conductivity. All results are solution-converged data based upon the energy residual, which becomes less than $10^{-18}$ to ensure a mature simulation. Text User Interface (TUI) of Fluent was used for different material properties and boundary conditions such as thickness. Most CFD codes provide journaling macro functions in the C-language. The TUI code is automatically generated for easier understanding regardless of users' proficiency. Figure 2 shows the pseudo-code for the macro function (Kim *et al.*, 2022).

### 2.2 Experimental set-up

To verify the CFD, the thermal resistance of the pure copper sheet ($\sim 400\,\text{W/mK}$) is also measured via experiments. Figure 3(a) is the schematic of the experimental set-up from the heater to the heat sink. Thicknesses of 1 mm, 2 mm and 3 mm and the heater sink area of $60 \times 60\,\text{mm}^2$ and $90 \times 90\,\text{mm}^2$ are used. Copper 101 sheet, which meets the specification of

> ➤ **Run macro loop**
>> **A. Open case 1**
>>> i. **Define material property for the FHP**
>>> ii. **Define boundary conditions**
>>> iii. **Run iteration**
>>> iv. **Export facet temperature averages**
>> **B. Repeat for all 10,799 cases**
> ➤ **End macro loop**

**Figure 2.**
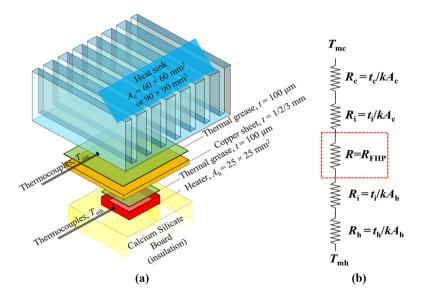Pseudo-code example



**Figure 3.**
(a) Schematic of experimental set-up; (b) Thermal resistance map of a FHP

(a)                                    (b)

ASTM F68, is used. Three cartridge heaters for a maximum power of 150 W each are embedded in a big copper block with a height of 50 mm to allow a uniform heating area of $25 \times 25$ mm$^2$. Power is fixed as 100 W, using a power supply. Insulation of the calcium silicate board is enclosed near the heater. Thermal greases (Tgrease, Laird) that is applied between the heat sink and the copper sheet, and the copper sheet and the heater are used for a close contact. It has a thermal conductivity of 1.2 W/mK, where the thermal resistance appears to be 0.01 K/W with a heat sink area of $90 \times 90$ mm$^2$ and a layer thickness of 100 $\mu$m (Moon *et al.*, 2021b).

A hole, 1 mm in diameter, is drilled at 5 mm from the surface of the heater and heat sink and three thermocouples are inserted to each to extrapolate $T_{mc}$ and $T_{mh}$. The temperatures are gathered by data acquisition systems (RDXL12SD, Omega) for 10 min to gain a steady state. The special limit of $T$-type thermocouples (TT-T-30-SLE-100, Omega) is used. The heatsink with a blower (VC-200, ATS) has the minimum thermal resistance of 0.2 K/W, and the heat transfer coefficient can be controlled up to 1,000 W/m$^2$K, with a power supply (GPR-3060D, Gwinstech). When repeated for ten times, the calculated maximum uncertainties in the reported temperature and thermal resistance values are 4.04% and 5.01%, respectively. Specifically, the measurement error for the thermocouples is 0.4%, and the change in the copper plate is 0.51%. Uncertainty of the input voltage and current uncertainty is 0.5%. Uncertainties are obtained by Moffat (Moffat, 1988):

$$\delta T = \sqrt{\sum_{i=1}^{n} \left( \frac{\partial T_i}{\partial x_i} \delta x_i \right)^2}$$

and

$$\delta R = \sqrt{\sum_{i=1}^{n} \left( \frac{\partial R}{\partial x_i} \delta x_i \right)^2}. \tag{3}$$
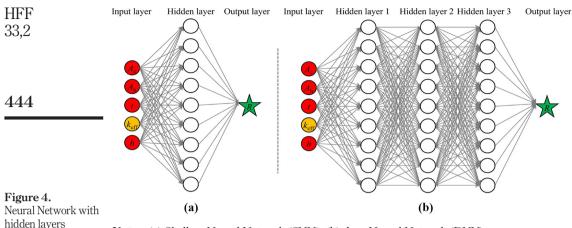
*2.3 Neural network regression*

To estimate the required effective thermal conductivity related to the spreading thermal resistance of the FHP, the Shallow or DNN approach is used with MATLAB via the Machine Learning ToolBox (MathWorks, 2022). Network structure, the activation function and the learning algorithm are the major components. The default neural network model has a structure shown in Figure 4. This leads to a certain number of inputs of $x = [A_c, A_h, k_{eff}, h]$ and a bias value $b$ (MathWorks, 2022; Tausendschøn and Radl, 2021; Lee *et al.*, 2020; Solgi *et al.*, 2017) for an output value $\hat{y}$. When an input layer is activated, it is calculated with a weight $w = [w_1, w_2, w_3, w_4, w_5]$. If a neuron has five inputs, it considers the same number of weights during learning time shown in equation (4). The activation function $f(z)$ should be able to handle the non-linear tendency of the data. This function gives the optimal value to reduce errors between 0 and 1, as shown in equation (5) below.

$$z = A_c{}^*w_1 + A_h{}^*w_2 + t^*w_3 + k_{eff}{}^*w_4 + h^*w_5 + b, \tag{4}$$

**Figure 4.**
Neural Network with
hidden layers

**Notes:** (a) Shallow Neural Network (SNN); (b) deep Neural Network (DNN)

$$\hat{y} = f(z). \tag{5}$$

There are many examples of an activation function, such as *ReLU* (rectified linear unit) in equation (6) or *Tanh* in equation (7), to obtain the appropriate output value of the spreading thermal resistance $R$ (MathWorks, 2022; Tausendschøn and Radl, 2021; Lee *et al.*, 2020; Solgi *et al.*, 2017). The application of the loss function, activation function, bias and weight for the output can be operated by Machine Learning Toolbox.

$$ReLU(z) = \begin{cases} 0 & \text{for} \quad z < 0 \\ z & \text{for} \quad z \geq 0 \end{cases}, \tag{6}$$

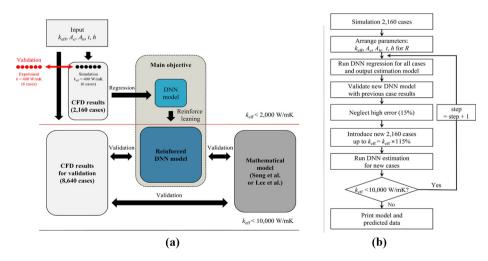$$Tanh(z) = \frac{2}{1 + e^{-2z}} - 1. \tag{7}$$

When learning the data, the activation functions should be chosen depending on the convergence and accuracy as the CFD results are non-linearly distributed (MathWorks, 2022; Tausendschøn and Radl, 2021; Lee *et al.*, 2020; Solgi *et al.*, 2017). In Figure 4, the input layer corresponds to the predictor data such as the effective thermal conductivity, heatsink area, heater area, thickness and heat transfer coefficient. The initial layer has resulted from 2,160 cases to the fully connected (FC) hidden layer, and it is judged by the activate function and filtered by the second or third FC layer to make an output of the spreading thermal resistance (MathWorks, 2022). A total of 3,000 iterations are performed to get a precise NN prediction. With the iterations of 1,000 and 2,000, the result fluctuates greatly, but in the case of 3,000 iterations, the data prediction converges to less than 0.3% deviation for several runs. The output value of the thermal resistance is returned by the weight or the biases in FC.

In Figure 4, the effect of the hidden layer on the neural network is shown. The SNN deals only with one hidden layer, and a premature convergence is expected. On the other hand, the DNN understands the complex non-linear pattern from the input and output layers considering the backpropagation. The non-linear tendency from input and output layers can

be validated in hidden layers (Chauhan *et al.*, 2019; Løhner *et al.*, 2021). As research on the thermal regression with the hidden layer effect have been lacking, this study will look at those afterwards. In the DNN, 50, 30, and 20 nodes are chosen for the first, second, and third layers, respectively, whereas the SNN has only 50 nodes.
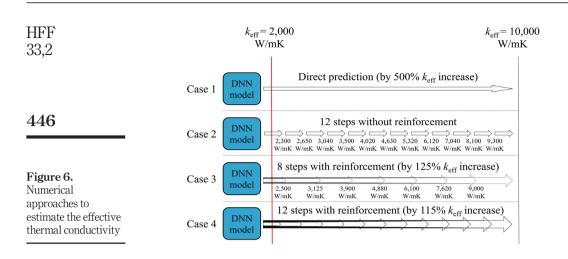
The prediction procedure in this study is shown in Figure 5(a) and 5(b). The first presents the prediction and validation procedure with the DNN. The CFD data with the effective thermal conductivity up to $k_{eff} = 2,000$ W/mK is completed to get the DNN regression. The initial input values in CFD are given in Table 1. The neural network model cannot generate a mathematical equation in MATLAB, but the output can return when the data is entered. The validation process for all data is made in each step. The average error between the original data and the prediction should be minimal for each step to ensure a minor deviation in the final step. As a large error or an outlier can exist, 15% of original data can be neglected in the next step to eliminate the possibility of greater errors in the next step. DNN regression is retrained for reinforcement learning to predict in a broader range based on the refined original data and the new one (Liu *et al.*, 2021). The newly introduced data should be in the broader range of the effective thermal conductivity above 15% to 25%.

Four approaches are shown in Figure 6. Case 1 is the direct prediction to $k_{eff} = 10,000$ W/mK by the neural network regression based on that $k_{eff} = 2,000$ W/mK. Case 2 is the prediction without reinforcement learning in twelve steps. In each step, the effective thermal conductivity increases by 15%. Case 3 uses the reinforcement by appending original data by 125% ($k_{eff} = k_{eff} \times 125\%$). Case 4 deals with more steps than Case 3 by appending original data by 115% ($k_{eff} = k_{eff} \times 115\%$). Finally, the case studies are validated with CFD results when $k_{eff} = 10,000$ W/mK or the correlation equation of Lee *et al.* (1995), Song *et al.* (1994). All first step uses the DNN regression for simulation data with the effective thermal conductivity ranging from 0 to 2,000 W/mK. The CFD by Fluent and the neural network algorithm by MATLAB are performed using Intel® Core™ i7 CPU with NVIDIA® 2060 Super GPU.



**Notes**: (a) Regression learning and validation from CFD data; (b) reinforcement learning example

**Figure 6.**
Numerical
approaches to
estimate the effective
thermal conductivity

## 3. Results and discussion
### 3.1 Spreading thermal resistance by computational fluid dynamics
For the flat heat pipe, it is known that the highest temperature of the heater is found at the center, and a lower temperature is measured at the heatsink, which has a broader area. When the heat flows, resistance changes as the size of the heatsink differs. This resistance is called spreading resistance or spreading thermal resistance (Lee *et al.*, 1995). It is assumed to be identical to the average value of the flat heat pipe (Lee *et al.*, 1995). The spreading thermal resistance can be defined as follows:

$$R = \left(\overline{T}_{\mathrm{h}} - \overline{T}_{\mathrm{c}}\right)/Q, \tag{8}$$

where $\overline{T}_{\mathrm{h}}$ and $\overline{T}_{\mathrm{c}}$ is the average temperature measured at the heater and heatsink, respectively. The $Q$ is the heat power of the heat source. Figure 7 depicts the effective thermal conductivity tendency with different spreading thermal resistance, thickness,
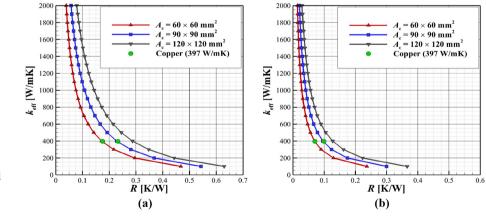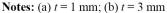


**Figure 7.**
Spreading thermal
resistance with
different heatsink
areas

**Notes:** (a) $t = 1$ mm; (b) $t = 3$ mm

and heatsink area. Results from simulations are based on the heat transfer coefficient of 1,000 W/m$^2$K of the heater area with the size of $25 \times 25$ mm$^2$. Effective thermal conductivity up to 2,000 W/mK is presented considering the reference values of aluminum, copper, and diamond: approximately 200 W/mK, 400 W/mK, and 2,000 W/mK, respectively. It is crucial to compare the spreading thermal resistance with that of copper and diamond for the range of flat heat pipe and the first regression.

Figure 7(a) and 7(b) show that the increase in effective thermal conductivity leads to a decrease in the spreading thermal resistance, indicating effective heat spread over the heat sink. Even though the spreading thermal resistance is the same, the high effective thermal conductivity makes a higher radial heat transfer. For example, when the spreading thermal resistance is 0.2 K/W and $t = 1$ mm, the effective thermal conductivity reaches 340 W/mK, 482 W/mK, and 668 W/mK for the heater area of $60 \times 60$ mm$^2$, $90 \times 90$ mm$^2$, and $120 \times 120$ mm$^2$, respectively. The effective thermal conductivity can also sharply rise with a drop in spreading thermal resistance. Between 0.2 K/W and 0.06 K/W when $A_c = 90 \times 90$ mm$^2$, the effective thermal conductivity can go up from 340 W/mK to 2,000 W/mK. When the thickness is larger because of internal structures like capillary wicks, the effective thermal conductivity can be decreased, which is not applicable and suitable. A similar tendency is found when $t = 1$ mm and $t = 5$ mm, as shown in Figure 7(a) and 7(b). It is proven that a larger heatsink area is required. In addition, the total thickness of the flat heat pipe should be as small as possible.

The spreading thermal resistance of the copper sheet ($R_{Cu}$) can be obtained by one-dimension conduction following equation (9).

$$R_{Cu} = \frac{T_{mh} - T_{mc}}{Q} - R_c - 2R_i - R_h = \frac{T_{mh} - T_{mc}}{Q} - \frac{t_c}{k_c A_c} - \frac{2t_i}{k_i A_i} - \frac{t_h}{k_{Al} A_{Al}} \tag{9}$$
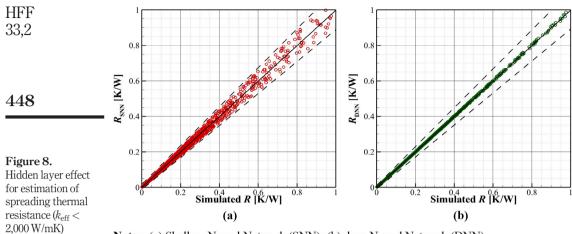
In Figure 7(a) and 7(b), the thermal resistance values by measurement are matched with the simulation data for different thicknesses and heatsink areas. In equations (1) and (2), the governing equation of CFD simulation is not complex and the accuracy of the simulation can be guaranteed. The spreading thermal resistance for $t = 2$ mm and $A_c = 60 \times 60$ mm$^2$ and $90 \times 90$ mm$^2$ for a copper sheet is 0.096 K/W and 0.14 K/W, respectively. Also, the simulation results for the same conditions are 0.096 K/W and 0.133 K/W, showing a good agreement. Therefore, an average difference of 1.5% can be found, considering the maximum uncertainty of 5.01%.

### 3.2 Hidden layer effect on neural network regression

Figure 8 shows the effect of the hidden layer on estimating the spreading thermal resistance. Instead of the effective thermal conductivity, comparing the spreading thermal resistance is more straightforward, as this parameter can be obtained by differing temperatures in experiments or via numerical analysis. The SNN and DNN with three hidden layers are compared in Figure 8(a) and 8(b), respectively. To compare the effect of the DNN accuracy, the mean absolute percentage error (*MAPE*) and the root mean square error (*RMSE*) are also compared as shown in equations (10) and (11) below:

$$MAPE = \frac{100}{N} \sum_{i=1}^{N} \left| \frac{y_i - \hat{y}_i}{y_i} \right|, \tag{10}$$

**Notes:** (a) Shallow Neural Network (SNN); (b) deep Neural Network (DNN)

$$RMSE = \sqrt{\sum_{i=1}^{N} (y_i - \hat{y}_i)^2 / N}, \tag{11}$$

where i is variable, $N$ is the number of data points, $y_i$ is simulation data, and $\hat{y}_i$ indicates the estimated value by DNN. The dashed line indicates the 10% *MAPE* from the simulation results. All neural network regression can fall in 10% error, and higher accuracy is found with DNN. The mean absolute percentage error of SNN and DNN is 6.9% and 1.1%, respectively.
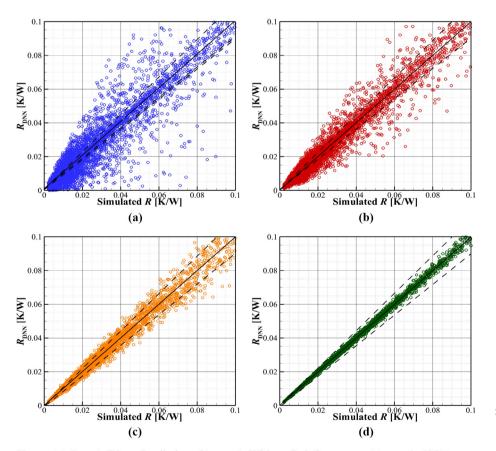
In particular, the activation function of *Tanh* is used, as the *ReLU* shows a poorer accuracy of 4.0% with the DNN. As the derivative of *ReLU* becomes monotonic, a classification issue arises because this activation function overfits the data among many simulation results (Astola *et al.*, 2021; Jamei *et al.*, 2021).

*RMSE* is found to be 0.0025 K/W and 0.0003 K/W for SNN and DNN, respectively, showing a higher prediction performance with DNN. It is well known that the *RMSE* can increase with the number of data points (Astola *et al.*, 2021). In the hidden layer, there is a loss function calculating the difference between the prediction value of the neural network model and the actual value. The neural network algorithm uses the loss value in backpropagation to correct the weight where it is made. The weight correction in nodes in layers of the neural network is called learning (Lim, 2020; Astola *et al.*, 2021). For reinforcement learning in this study, the loss values can be reduced in advance by removing data that greatly deviate by approximately 15% in each step in the DNN. In addition, the previous data to be regressed is always larger than the new data to be learned, therefore the prediction does not deviate much in this study.

Therefore, the loss values can drop with a rise in the number of layers. However, having four or more hidden layers is not recommended as discussed in Lim (2020) as it can overfit the training data. The optimal number of hidden layers should be carefully chosen for a higher accuracy.

*3.3 Estimation and validation of deep neural network*

Figure 9 shows several neural network methods to obtain an accurate prediction up to when $k_{eff} = 10,000$ W/mK. Simulation data for the same independent variables are used for the validation. All graphs are presented for the range between 0.001 K/W and 0.1 K/W, as it covers the range of effective thermal conductivity from 2,000 W/mK to 10,000 W/mK. This study compares 8,640 simulation results under the same input conditions. The graph indicates the accuracy of different prediction approaches. In Figure 9(a) of case 1, the direct prediction of $k_{eff} = 2,000$ W/mK from the regressed model shows a poor estimation up to 500% error. Most data does not fit in the 10% deviation, and the estimated value can be negative. As regression is carried out for the small ranges, the prediction cannot be used directly for values higher by five or more times. Even though the regression shows a good fit, the bias and weight are learned by local input values, making a higher deviation in estimation. In Figure 9(b), the prediction without reinforcement learning is still poor, and the tendency is quite different from Figure 9(a). In this case, the first step shows a deviation of only 1.1% from simulated data when $k_{eff}$ goes up to 2,300 W/mK. The deviation



**Notes**: (a) Case 1: Direct Prediction; (b) case 2: Without Reinforcement; (c) case 3: 125% Reinforcement; (d) case 4: 115% Reinforcement
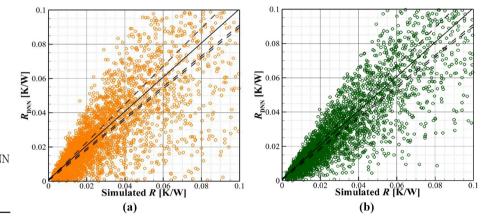
**Figure 9.**
Several deep neural network prediction approaches to estimate $k_{eff} <$ 10,000 W/mK

exponentially increases and backpropagation fails, leading to a overfit in the final step. Case 3 and 4 in Figure 9(c) and 9(d) show more accurate results with near 10% deviation, showing the effect of reinforcement learning.

The learning process may be effective, but a higher accuracy can be found with 115% reinforcement, as shown in Case 4. The first estimation shows the same deviation of 1.1% in Case 2. The error does not deviate much in steps and maintains a low estimation value, showing an excellent performance up to $k_{eff} < 10,000$ W/mK. Even with reinforcement learning, outliers can be found, but reliable data will appear with a higher prediction accuracy.

Figure 10 shows the SNN to estimate $k_{eff} < 10,000$ W/mK. Reinforcements of 25% and 15% by SNN are also presented. However, an average error of up to 35% can be found even with the 15% reinforcement. Even though 15% of error has been removed in each step, still all existing data are predicted with a significant deviation. This is because the errors have been accumulated in every step due to SNN. Therefore, a minimal handling error of around 1% is required as shown in Figure 8(b) to ensure estimation accuracy. Also, a number of data should be ensured for accuracy.

Figure 11 shows the *MAPE* for each step up to $k_{eff} = 10,000$ W/mK. From the DNN regression, all twelve steps are presented. All calculated data can be controlled in 10% line,



**Figure 10.**
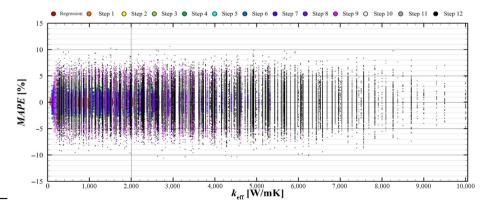SNN prediction approaches to estimate $k_{eff} < 10,000$ W/mK by SNN with (a) 25% reinforcement (b) 15% reinforcement



**Figure 11.**
*MAPE* for each step for 15% reinforcement of DNN

due to reinforcement learning. The effective thermal conductivity up to 2,000 W/mK should be learned in every step to ensure the accuracy of the DNN estimation. The increasing error trend for each step is inevitable because of an increase in uncertainty. This can be solved by reducing the size of each step. However, if it is reduced, the amount of data that needs to be learned increases, taking more time to compute which is not feasible. Therefore, it is necessary to select an optimal size of each step and data amount to keep the computation time to a minimum while maintaining the standard of uncertainty to be less than 10%.

*3.4 Theoretical model comparison*
DNN prediction model validated with simulations is compared again with the analytical model in Lee *et al.* (1995). For square-shaped heat pipes, the equivalent heat source diameter $d_h$ and heatsink diameter $d_c$ can be obtained:

$$d_h = \sqrt{\frac{A_h}{\pi}} \tag{12}$$

$$d_c = \sqrt{\frac{A_c}{\pi}} \tag{13}$$

where $A_h$ is the heater area, and $A_c$ is the heatsink area. The spreading thermal resistance of the flat heat pipe can be calculated by the correlation below:

$$R = \frac{\frac{\varepsilon\tau}{\sqrt{\pi}} + \frac{1}{2}(1-\varepsilon)^{1.5}\Phi}{\sqrt{\pi}k_{eff}d_h} \tag{14}$$

$$\Phi = \frac{\tanh(\lambda\tau) + \frac{\lambda}{Bi}}{1 + \frac{\lambda}{Bi}\tanh(\lambda\tau)} \tag{15}$$

where $\lambda = \pi + 1/(\sqrt{\pi}\varepsilon)$, and $\varepsilon$ is the dimensionless radius ($= d_h/d_c$). $\tau$ is the thickness of the dimensionless plate ($= t/d_c$). The Biot number is proposed for the conduction and convective heat transfer in equation (16) as follows:

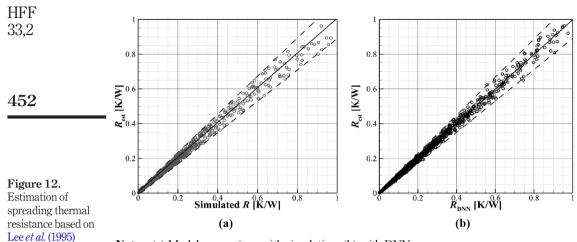$$Bi = \frac{hd_c}{k_{eff}} \tag{16}$$

This model has an accuracy of approximately 10% in estimating the effective thermal conductivity using a heatsink for conventional metals (Lee *et al.*, 1995). If the spreading thermal resistance is known, the effective thermal conductivity can be calculated with an inverse function shown below:

$$k_{eff} = g^{-1}(R). \tag{17}$$

For the 10,800 simulation cases, the simulation results and the DNN regression model are compared with the same dependent variables with the equation (14) and the outcomes are shown in Figure 12(a) and 12(b). In equation (14), the model works when the heatsink area is larger than the heater area ($A_c > A_h$). The *MAPE* of 10.8% and 9.7% are found in

Figure 12.
Estimation of
spreading thermal
resistance based on
Lee *et al.* (1995)

**Notes:** (a) Model comparison with simulation; (b) with DNN

Figure 12(a) and 12(b). The DNN results show a better estimation when compared to the simulation. Above 90% of the data is bounded by a 10% deviation line for two validation methods. In addition, the partial ranges up to $k_{eff} < 2,000$ W/mK shown in Figures 8 and 9 have a good agreement. During the steps shown in Figure 11, all results fitted within 10% with equation (17).

Therefore, the DNN estimation using reinforcement learning helps to predict the effective thermal conductivity. This method can estimate from known values by filtering non-predictable data and controlling minor errors. Even though the current study does not consider the effect of data amount, it is necessary to investigate the relation between the number of hidden layers, step size, and reinforcement learning approach for various thermal issues. With DNN, the effective thermal conductivity can be estimated by obtaining the spreading thermal resistance. Table 2 shows the summarized results via DNN, assuming $h = 1,000$ W/m$^2$K, $A_h = 10 \times 10$ mm$^2$, and $A_c = 90 \times 90$ mm$^2$. There is a small difference between the simulations and DNN results under the same condition. The regression and the reinforced DNN model appropriately proceed to estimate the effective thermal conductivity of the flat heat pipe. Another advantage of DNN is that it can significantly reduce

|  |  | DNN results at $A_c = 90 \times 90$ mm$^2$ and $A_h = 10 \times 10$ mm$^2$ | | | | | | Simulated results |
|  | $t$ [mm] | 0.5 | 1 | 2 | 3 | 4 | 5 | 1 |
| Category | $k_{eff}$ [W/mK] | | | | $R$ [K/W] | | | |
| Regressed DNN | 200 | 1.478 | 0.914 | 0.549 | 0.412 | 0.342 | 0.302 | 0.914 |
|  | 400 | 0.900 | 0.524 | 0.298 | 0.218 | 0.178 | 0.155 | 0.525 |
|  | 2,000 | 0.231 | 0.122 | 0.065 | 0.046 | 0.037 | 0.032 | 0.122 |
| Reinforced DNN | 3,000 | 0.158 | 0.082 | 0.043 | 0.031 | 0.025 | 0.021 | 0.082 |
| (prediction) | 4,000 | 0.120 | 0.062 | 0.033 | 0.023 | 0.019 | 0.016 | 0.062 |
|  | 7,000 | 0.070 | 0.036 | 0.019 | 0.013 | 0.011 | 0.009 | 0.036 |
|  | 8,000 | 0.062 | 0.031 | 0.016 | 0.012 | 0.009 | 0.008 | 0.031 |
|  | 10,000 | 0.049 | 0.025 | 0.013 | 0.009 | 0.007 | 0.006 | 0.025 |

Table 2.
Effective thermal
conductivity by
spreading thermal
resistance obtained
by DNN

computation time. With MATLAB, the calculation takes less than 8 h with 10–75 min for each step, whereas CFD takes 260 h to calculate 8,640 cases with Fluent for the same parallel computing. Having a similar accuracy, there is a big difference in the computational efficiency.

## 4. Conclusions
This study uses the DNN algorithm to investigate the effective thermal conductivity estimation for flat heat pipes with different conditions. The conclusions are as follows:

- Big data by CFD are established for the effective thermal conductivity up to 2,000 W/mK. Flat heat pipes with different heatsink areas, heater areas, heat transfer coefficients and thicknesses are numerically studied. The validations are made between experiments and simulations for the copper solid.

- The effect of the hidden layers is also examined by comparing the SNN and DNN with the big data. While both show an acceptable accuracy, the DNN is found to be more advantageous with backpropagation.

- The effective thermal conductivity with different spreading thermal resistance is estimated up to 10,000 W/mK by using the DNN. Reinforcement learning maintains fewer errors by removing the worst 15% of data in each step. By comparing the simulation results, theory from other literature and the DNN approach to validate the effective thermal conductivity up to 10,000 W/mK, we can conclude that the DNN estimation is practical. In addition, DNN regression and estimation can open new ways to secure data while making predictions in a wide range without conducting experiments or simulations.

## References

ANSYS (2022), "Fluent user guide".

Astola, H., Seitsonen, L., Halme, E., Molinier, M. and LøNNQVIST, A. (2021), "Deep neural networks with transfer learning for forest variable estimation using sentinel-2 imagery in boreal Forest", *Remote Sensing*, Vol. 13 No. 12.

BAR-Cohen, A., Matin, K., Jankowski, N. and Sharar, D. (2015), "Two-phase thermal ground planes: technology development and parametric results", *Journal of Electronic Packaging*, Vol. 137 No. 1.

Chang, F.L. and Hung, Y.M. (2019), "Gravitational effects on electroosmotic flow in micro heat pipes", *International Journal of Numerical Methods for Heat and Fluid Flow*, Vol. 30 No. 2, pp. 535-556.

Chauhan, S., Vig, L., DE Filippo, D.E., Grazia, M., Corbetta, M., Ahmad, S. and Zorzi, M. (2019), "A comparison of shallow and deep learning methods for predicting cognitive performance of stroke patients from MRI lesion images", *Frontiers in Neuroinformatics*, Vol. 13, p. 53.

Chen, G., Tang, Y., Wan, Z., Zhong, G., Tang, H. and Zeng, J. (2019), "Heat transfer characteristic of an ultra-thin flat plate heat pipe with surface-functional wicks for cooling electronics", *International Communications in Heat and Mass Transfer*, Vol. 100, pp. 12-19.

Jamei, M., Olumegbon, I.A., Karbasi, M., Ahmadianfar, I., Asadi, A. and Mosharaf-Dehkordi, M. (2021), "On the thermal conductivity assessment of Oil-Based hybrid nanofluids using extended kalman filter integrated with feed-forward neural network", *International Journal of Heat and Mass Transfer*, Vol. 172.

Jiang, B.T. and Zhao, F.Y. (2013), "Combination of support vector regression and artificial neural networks for prediction of critical heat flux", *International Journal of Heat and Mass Transfer*, Vol. 62, pp. 481-494.

Kim, M., Lee, K.H., Han, D.I. and Moon, J.H. (2022), "Numerical case study and modeling for spreading thermal resistance and effective thermal conductivity for flat heat pipe", *Case Studies in Thermal Engineering*, Vol. 31.

Lee, S., Song, S., Au, V. and Moran, K. (1995), "Constriction/spreading resistance model for electronics packaging", *ASME/JSME Thermal Engineering Conference*, pp. 199-206.

Lee, S., Cho, S., Kim, S.-H., Kim, J., Chae, S., Jeong, H. and Kim, T. (2020), "Deep neural network approach for prediction of heating energy consumption in old houses", *Energies*, Vol. 14 No. 1, p. 122.

Lewis, R.W. (2004), *Fundamentals of the Finite Element*, Wiley, New York, NY.

Lewis, R.W. (2016), *Fundamentals of the Finite Element Method for Heat and Mass Transfer*, Wiley, New York, NY.

Lewis, R.W. and Sukirman, Y. (1994), "Finite element modelling for simulating the surface subsidence above a compacting hydrocarbon reservoir", *International Journal for Numerical and Analytical Methods in Geomechanics*, Vol. 18 No. 9, pp. 619-639.

Lewis, R.W., Morgan, K., Thomas, H.R. and Seetharamu, K.N. (1996), *The Finite Element Method in Heat Transfer Analysis*, John Wiley and Sons, New York, NY.

Lim, H.-I. (2020 ), "A study on layers of deep neural networks", *3rd International Conference on Intelligent Autonomous Systems (ICoIAS)*, Singapore, IEEE, pp. 1-18.

Liu, W., Gou, J., Luo, Y. and Zhang, M. (2018), "The experimental investigation of a vapor chamber with compound columns under the influence of gravity", *Applied Thermal Engineering*, Vol. 140, pp. 131-138.

Liu, T., Li, Y., Jing, Q., Xie, Y. and Zhang, D. (2021), "Supervised learning method for the physical field reconstruction in a nanofluid heat transfer problem", *International Journal of Heat and Mass Transfer*, Vol. 165.

Løhner, R., Antil, H., Tamaddon-Jahromi, H., Chakshu, N.K. and Nithiarasu, P. (2021), "Deep learning or interpolation for inverse modelling of heat and fluid flow problems?", *International Journal of Numerical Methods for Heat and Fluid Flow*, Vol. 31 No. 9, pp. 3036-3046.

Mathworks (2022), "Matlab documentation".

Moffat, R.J. (1988), "Describing the uncertainties in experimental results", *Experimental Thermal and Fluid Science*, Vol. 1 No. 1, pp. 3-17.

Moon, J.H., Choi, C.K. and Lee, S.H. (2021a), "Local mass flux and pinning behavior of an evaporating droplet on heated aluminum surfaces", *Case Studies in Thermal Engineering*, Vol. 26, p. 101171.

Moon, J.H., Fadda, D., Shin, D.H., Kim, J.S., Lee, J. and You, S.M. (2021b), "Boiling-driven, wickless, and orientation-independent thermal ground plane", *International Journal of Heat and Mass Transfer*, Vol. 167, p. 120817.

Navti, S.E., Ravindran, K., Taylor, C. and Lewis, R.W. (1997), "Finite element modelling of surface tension effects using a Lagrangian-Eulerian kinematic description", *Computer Methods in Applied Mechanics and Engineering*, Vol. 147 No. 1-2, pp. 41-60.

Solgi, M., Najib, T., Ahmadnejad, S. and Nasernejad, B. (2017), "Synthesis and characterization of novel activated carbon from medlar seed for chromium removal: experimental analysis and modeling with artificial neural network and support vector regression", *Resource-Efficient Technologies*, Vol. 3 No. 3, pp. 236-248.

Song, S., Lee, S. and Au, V. (1994), "Closed-Form equation for thermal constriction/spreading resistance with variable resistance boundary condition", *International Electronics Packaging Conference*, pp. 111-121.

Tausendschøn, J. and Radl, S. (2021), "Deep neural network-based heat radiation modelling between particles and between walls and particles", *International Journal of Heat and Mass Transfer*, Vol. 177.

Teimouri, H. and Behzadmehr, A. (2020), "Effects of magnetic field on the liquid gallium thermosyphon fluid flow; a numerical study", *International Journal of Numerical Methods for Heat and Fluid Flow*, Vol. 30 No. 2, pp. 681-703.

Tsai, M.-C., Kang, S.-W. and Vieira DE Paiva, K. (2013), "Experimental studies of thermal resistance in a vapor chamber heat spreader", *Applied Thermal Engineering*, Vol. 56 Nos 1/2, pp. 38-44.

Wang, J.C. (2010), "Development of vapour chamber-based VGA thermal module", *International Journal of Numerical Methods for Heat and Fluid Flow*, Vol. 20 No. 4, pp. 416-428.

Yang, Y., L.I., J., Wang, H., Liao, D. and Qiu, H. (2021), "Microstructured wettability pattern for enhancing thermal performance in an ultrathin vapor chamber", *Case Studies in Thermal Engineering*, Vol. 25.

Zhou, F., Liu, Y. and Dede, E.M. (2019), "Design, fabrication, and performance evaluation of a hybrid wick vapor chamber", *Journal of Heat Transfer*, Vol. 141 No. 8.

Zhu, M., Huang, J. and Song, M.H.U., Y. (2020), "Thermal performance of a thin flat heat pipe with grooved porous structure", *Applied Thermal Engineering*, Vol. 173.

**Corresponding author**

Joo Hyun Moon can be contacted at: jhmoon9@sejong.ac.kr